

Triangulation of gravitational wave sources with a network of detectors

Stephen Fairhurst

Cardiff School of Physics and Astronomy, Cardiff University, Queens Buildings,
The Parade, Cardiff. CF24 3AA

E-mail: Stephen.Fairhurst@astro.cf.ac.uk

Abstract.

There is significant benefit to be gained by pursuing multi-messenger astronomy with gravitational wave and electromagnetic observations. In order to undertake electromagnetic follow-ups of gravitational wave signals, it will be necessary to accurately localize them in the sky. Since gravitational wave detectors are not inherently pointing instruments, localization will occur primarily through triangulation with a network of detectors. We investigate the expected timing accuracy for observed signals and the consequences for localization. In addition, we discuss the effect of systematic uncertainties in the waveform and calibration of the instruments on the localization of sources. We provide illustrative results of timing and localization accuracy as well as systematic effects for coalescing binary waveforms.

1. Introduction

There is a growing realization that multi-messenger astronomy will be of critical importance for gravitational wave astronomy. While the concept has been discussed for many years (e.g. [1]), only recently has a large push towards joint observations with electromagnetic and neutrino detectors begun (see e.g. [2, 3, 4, 5]). Initially, joint observations will provide additional confidence for early detections made in non-stationary gravitational wave data. Later, multi-messenger observations will be critical in extracting the maximum scientific payoff from gravitational wave observations. For example, the cleanest way to demonstrate that the progenitors of short γ -ray bursts (GRBs) are coalescing Neutron stars would be the observation of a gravitational wave chirp associated with a short GRB [6]. Additionally, joint observations will likely provide measurements of complementary parameters, thereby breaking degeneracies which would exist with single messenger observations.

The road to joint observations has already been paved, with several gravitational wave search results being “triggered” by external observations, such as GRBs [7, 8] and soft gamma repeaters [9, 10]. More recently, work has begun to ensure that gravitational wave observations can be followed up by other astronomical observatories. In the era of regular gravitational wave observations, it is likely that gravitational wave alerts will be followed up by large field of view optical (such as Pan Starrs [11]), γ -ray (Swift [12], Fermi [13]) and radio observatories (Lofar[14, 15]) as well as neutrino observatories (Ice Cube [16], Antares [17]).

The vast majority of electromagnetic observatories are, by their very nature, directional. Thus, in order for gravitational wave observations to be useful to other astronomers, it is necessary to extract the sky location from the gravitational wave signal. However, gravitational wave detectors are sensitive to signals from large fraction of the sky and a single gravitational wave detector provides essentially no directional information for a short duration source. Thus, the ability to reconstruct the location of a transient signal is primarily due to triangulation based on the observed time delays of the signal at several detectors. For more than two sites, requiring a consistency between the observed amplitudes will also serve to restrict the allowed sky positions. In particular, for three detectors, using only timing information, one obtains two sky locations which are mirror images with respect to the plane of the three detectors; generically the amplitude information can be used to break this degeneracy. The issue of localization of gravitational wave signals with a detector network has been discussed previously, and several different algorithms proposed [18, 19, 20, 21, 22, 23, 24, 25, 26, 27].

In this paper, we consider the ability of gravitational wave detectors to localize transient signals by considering only the timing information available at each site. For concreteness, we restrict attention to elliptically polarized gravitational waves, a choice motivated by coalescing binary waveforms. With this simple model, we obtain a straightforward estimate for the expected timing accuracy and use this to evaluate the triangulation ability of a network of detectors. From timing information alone, it is only possible to measure the projection of the sky location onto the detector baseline. Thus for two detectors, localization to a ring in the sky is possible, while for three detectors a reflection degeneracy in the plane of the detectors remains.

In a gravitational wave search, there are several sources of uncertainties which will affect the localization ability of the search. First, when performing a matched filter search, there will typically be several additional parameters in the waveform model (such as the masses of a compact binary). These additional parameters will serve to degrade the localization ability. In addition, there are likely to be differences between the physical waveforms and the templates used. These arise due to errors in the waveform family due to truncation of analytic expansions or numerical inaccuracies. While the inaccuracies of the waveform are independent of the detector, their effect on the timing accuracy will depend upon detector sensitivity. Finally, there are uncertainties in the calibration of the detectors. These will result in the reconstructed gravitational wave strain $h(t)$ differing from the actual gravitational wave signal. These calibration uncertainties will have a similar effect to the use of an incorrect waveform template. However, the calibration inaccuracies, as well as the associated timing errors, will be largely independent in the different detectors.

The layout of the paper is as follows. In Section 2, we describe the restriction to elliptical polarization and briefly review the coalescing binary waveform. In Section 3 we obtain the expected timing accuracies, and in Section 4 present the localization ability of the network. Finally, in Section 5, we discuss the systematic uncertainties and their effect on timing. Throughout, we provide an illustrative example of expected results for binary neutron star (BNS) and binary black hole (BBH) systems.

2. The waveform model

In this paper, we will focus primarily on waveforms generated during binary coalescence. However, much of the framework introduced is applicable to a broader

class of waveforms. Therefore, we begin by laying out the minimal set of assumptions that are made on the form of the gravitational wave, before moving on to describe the waveform for binary neutron star and black hole coalescences in more detail.

We restrict attention to elliptically polarized waveforms, following a definition proposed by Sutton and Poprocki [28]. Specifically, a waveform is said to be elliptically polarized if there exists a polarization frame such that the two polarizations h_+ and h_\times of the gravitational wave are related by

$$h_+(t) = \eta_+ \alpha(t) \cos \varphi(t), \quad h_\times(t) = \eta_\times \alpha(t) \sin \varphi(t), \quad (1)$$

where $\alpha(t)$ and $\varphi(t)$ are the amplitude and phase of the waveform and $\eta_{+,\times}$ encode the relative amplitudes of the two polarizations. We make the additional requirement that the amplitude is slowly varying (with respect to the phase), i.e. $\dot{\alpha}/\alpha \ll \dot{\varphi}$. Then, in Fourier space, the two polarizations are related by

$$\tilde{h}_\times(f) = i\eta \tilde{h}_+(f). \quad (2)$$

where $\eta \in [-1, 1]$ provides the ratio between the two amplitudes, with unity corresponding to circular polarization and zero to linear polarization.

The gravitational waveform observed at a detector can be expressed as

$$h(t) = F_+(\theta, \phi, \psi) h_+(t; \boldsymbol{\xi}) + F_\times(\theta, \phi, \psi) h_\times(t; \boldsymbol{\xi}) \quad (3)$$

Here, F_+ and F_\times are the well known detector response functions (see e.g. [29]) which depend upon the sky location (θ, ϕ) of the system relative to the detector and the polarization ψ . We use $\boldsymbol{\xi}$ to denote any additional parameters upon which the waveform depends. It follows straightforwardly from (2) and (3) that the gravitational waveform observed in a given detector can be expressed as:[‡]

$$h(t) = A_0 h_0(t; \boldsymbol{\xi}) + A_{\frac{\pi}{2}} h_{\frac{\pi}{2}}(t; \boldsymbol{\xi}) \quad (4)$$

where

$$\tilde{h}_{\frac{\pi}{2}}(f; \boldsymbol{\xi}) = i\tilde{h}_0(f; \boldsymbol{\xi}). \quad (5)$$

The constants A_0 and $A_{\frac{\pi}{2}}$ depend upon the location of the source relative to the detector and the parameter η introduced above. Finally, we write the waveform explicitly in terms of amplitude and phase as

$$\tilde{h}_0(f; \boldsymbol{\xi}) = A(f; \boldsymbol{\xi}) e^{i\Phi(f; \boldsymbol{\xi})} \quad \text{and} \quad \tilde{h}_{\frac{\pi}{2}}(f; \boldsymbol{\xi}) = iA(f; \boldsymbol{\xi}) e^{i\Phi(f; \boldsymbol{\xi})}. \quad (6)$$

2.1. Waveforms for Coalescing Binaries

For concreteness, let us now specialize to the waveform emitted during binary coalescence, where we neglect the spin of the two components. Then, the orbital plane will not precess and the two polarizations of the waveform can be expressed as [30]

$$\begin{aligned} h_+(t) &= \left(\frac{D_o}{D} \right) \left[\begin{array}{l} (1/2)(1 + \cos^2 \iota) \cos 2\phi_o h_0(t; t_o, D_o, m_1, m_2) \\ - \cos \iota \sin 2\phi_o h_{\frac{\pi}{2}}(t; t_o, D_o, m_1, m_2) \end{array} \right], \\ h_\times(t) &= \left(\frac{D_o}{D} \right) \left[\begin{array}{l} (1/2)(1 + \cos^2 \iota) \sin 2\phi_o h_0(t; t_o, D_o, m_1, m_2) \\ + \cos \iota \cos 2\phi_o h_{\frac{\pi}{2}}(t; t_o, D_o, m_1, m_2) \end{array} \right]. \end{aligned} \quad (7)$$

Here, D is the distance at which the signal is located, D_o is a fiducial distance (e.g. 1 Mpc), t_o and ϕ_o are a reference time and phase for the signal (often taken as the

[‡] We make use of the two ‘‘phases’’ of the waveform h_0 and $h_{\frac{\pi}{2}}$ as these arise naturally in the context of coalescing binaries, as we shall see in Section 2.1

coalescence time and phase), ι is the inclination angle of the binary relative to the line of sight and m_1 and m_2 are the masses of the binary's components. The two phases h_0 , $h_{\frac{\pi}{2}}$ are the waveforms, normalized for a binary at distance D_o , and depend upon the masses of the components as well as the coalescence time t_o .

The amplitude and phase of the waveform have been calculated to exquisite accuracy through the post-Newtonian expansion. Although the post-Newtonian expressions formally extend to infinite frequency, the waveform is truncated at a pre-specified frequency, typically the innermost stable circular orbit (ISCO). At higher frequencies, the finite size of the objects will cause the true waveform to differ significantly from the post-Newtonian expression. Furthermore, in many applications, the restricted post-Newtonian approximation is used where only the leading order amplitude term is used, while the phase is evaluated to higher post-Newtonian order. It is only the restricted post-Newtonian waveform which can be written in the form (6). The amplitude satisfies $A(f) \propto f^{-7/6}$ while the detailed phasing evolution will depend critically upon the masses of the system [31]. This waveform is appropriate for low mass binaries as the merger occurs at a higher frequency than the sensitive band of the detectors. We will illustrate the results in the remainder of the paper with numbers appropriate for a BNS signal with component masses $1.4M_{\odot}$ and an ISCO frequency of 1500 Hz.

More recently, breakthroughs in numerical relativity have allowed for the calculation of entire binary black hole merger waveform [32]. Work remains ongoing to cover the full mass and spin parameter space. However, for non-spinning binaries with comparable mass components, the waveform is well understood (see, e.g. [33, 34, 35, 36, 37]). Indeed, a phenomenological fit to these waveforms has been produced in [38]. Here, the inspiral waveform extends beyond the ISCO to a merger frequency, after which point the amplitude evolves as $A(f) \propto f^{-2/3}$, and finally incorporates a ringdown. For $10 - 10M_{\odot}$ waveforms, the ISCO is at 220 Hz, but the phenomenological waveform continues up to 800 Hz. We will show that, by including the merger and ringdown information, the timing and localization accuracies for these waveforms can be improved dramatically.

3. Timing Accuracy

The parameter estimation problem has been discussed in detail in many articles. Here, we provide a brief overview of the method in order to fix notation, (for further details, see e.g. [39]). We then proceed to use the framework to address the specific problem of timing accuracy. In later sections, we make use of the same framework to obtain localization estimates and address systematic uncertainties.

3.1. Parameter Estimation and the Fisher Matrix

In order to decide whether there is a signal present in the data, we calculate the likelihood ratio of a signal h parametrized by some set $\boldsymbol{\mu}$ of parameters[§] being present in the data s , relative to the null hypothesis:

$$\Lambda(\boldsymbol{\mu}) = \frac{p(s|h(\boldsymbol{\mu}))}{p(s|0)} = \frac{e^{-\langle s-h(\boldsymbol{\mu})|s-h(\boldsymbol{\mu}) \rangle/2}}{e^{-\langle s|s \rangle/2}}, \quad (8)$$

[§] e.g. for the coalescing binary signal introduced in section 2.1, $\boldsymbol{\mu} = (m_1, m_2, t_o, D, \theta, \phi, \psi, \iota, \phi_o)$.

where the inner product is defined as

$$\langle a|b \rangle = 4 \operatorname{Re} \int_0^\infty df \frac{\tilde{a}(f)\tilde{b}^*(f)}{S(f)}, \quad (9)$$

and $S(f)$ is the noise power spectrum of the detector. The formalism can be used both for the purposes of detection and parameter estimation, as described in e.g. [40]. For parameter estimation, we are interested in the posterior probability distribution of the parameters $\boldsymbol{\mu}$, given the data s . The posterior distribution for the parameters $\boldsymbol{\mu}$ can be obtained using Bayes' theorem as:

$$p(\boldsymbol{\mu}|s) = \frac{p(\boldsymbol{\mu})p(s|\boldsymbol{\mu})}{\int d\boldsymbol{\mu} p(\boldsymbol{\mu})p(s|\boldsymbol{\mu})} = \frac{p(\boldsymbol{\mu})\Lambda(\boldsymbol{\mu})}{\int d\boldsymbol{\mu} p(\boldsymbol{\mu})\Lambda(\boldsymbol{\mu})} \quad (10)$$

where $p(\boldsymbol{\mu})$ is the prior distribution on the parameters $\boldsymbol{\mu}$ and $\Lambda(\boldsymbol{\mu})$ is the likelihood ratio introduced above. If we are only interested in a subset $\boldsymbol{\xi}$ of the parameters $\boldsymbol{\mu}$ and not $\boldsymbol{\nu}$, we simply marginalize over the ‘‘nuisance’’ parameters $\boldsymbol{\nu}$ by integrating over them.

Let us now specialise to the case discussed in Section 2 where the waveform is parametrized by two orthogonal phases h_0 and $h_{\frac{\pi}{2}}$ satisfying (5), with arbitrary amplitudes A_0 and $A_{\frac{\pi}{2}}$ as in (4), and substitute this waveform into the expression (8) for the likelihood. The expression is simplified by noting that the two phases are necessarily orthogonal,

$$\langle h_0(\boldsymbol{\xi})|h_0(\boldsymbol{\xi}) \rangle = \langle h_{\frac{\pi}{2}}(\boldsymbol{\xi})|h_{\frac{\pi}{2}}(\boldsymbol{\xi}) \rangle \quad \text{and} \quad \langle h_0(\boldsymbol{\xi})|h_{\frac{\pi}{2}}(\boldsymbol{\xi}) \rangle = 0. \quad (11)$$

Finally, by either maximizing the likelihood with respect to A_0 and $A_{\frac{\pi}{2}}$ or by marginalizing over them with a uniform prior,^{||} we obtain

$$\ln \Lambda(\boldsymbol{\xi}) = \frac{\langle s|h_0(\boldsymbol{\xi}) \rangle^2 + \langle s|h_{\frac{\pi}{2}}(\boldsymbol{\xi}) \rangle^2}{2\langle h_0(\boldsymbol{\xi})|h_0(\boldsymbol{\xi}) \rangle}. \quad (12)$$

For other parameters, it is not possible to handle the marginalization of the likelihood so straightforwardly. Therefore, we make use of the Fisher Information Matrix to obtain expected parameter estimation accuracies. Briefly, assume that there is a signal in the data of the form

$$s = A_0 h_0(\boldsymbol{\xi}) + A_{\frac{\pi}{2}} h_{\frac{\pi}{2}}(\boldsymbol{\xi}) + n. \quad (13)$$

Further, assume that the amplitude of the signal is sufficiently large that the noise contribution n can be neglected. Then, expand the likelihood in the neighbourhood of the true signal parameter in powers of $d\boldsymbol{\xi}$. Setting $\langle h_0(\boldsymbol{\xi})|h_0(\boldsymbol{\xi}) \rangle = 1$ we obtain

$$\ln \Lambda(d\boldsymbol{\xi}) \approx \frac{\rho^2}{2} [1 - g_{ab} d\xi^a d\xi^b] \quad (14)$$

where $\rho^2 = (A_0^2 + A_{\frac{\pi}{2}}^2)$ and

$$g_{ab} = \langle \partial_a h_0 | \partial_b h_0 \rangle - \langle h_0 | \partial_a h_0 \rangle \langle h_0 | \partial_b h_0 \rangle - \langle h_{\frac{\pi}{2}} | \partial_a h_0 \rangle \langle h_{\frac{\pi}{2}} | \partial_b h_0 \rangle, \quad (15)$$

is a positive definite matrix. At quadratic order, the likelihood function is approximated as a multi-variate Gaussian around the peak $d\boldsymbol{\xi} = 0$. The Fisher matrix g_{ab} then provides an estimate of the accuracy with which the parameters $\boldsymbol{\xi}$ can, in principle, be determined.

^{||} In many cases, the sources of interest are approximately uniformly distributed in volume. This leads to a prior on the amplitude of A^{-4} . A uniform prior is chosen here for ease of calculation. For observed signals, the amplitude will be large enough that the choice of prior will not have a substantial effect on the parameter accuracy estimates derived later.

3.2. Timing

It is rather straightforward to utilize the formalism introduced above to investigate the effects of a timing error. In particular, restrict attention to the case where the parameter space ξ is the one dimensional time parameter. In this case, a shift of the time t_o corresponds to (frequency dependent) phase shift in the waveform and has no effect on the amplitude of the waveform, specifically

$$\tilde{h}_0(f; t_o + dt) = e^{2\pi i f dt} \tilde{h}_0(f; t_o). \quad (16)$$

We can obtain a posterior distribution for the timing error, making use of the formalism introduced above. Generally, the time will not be known apriori, certainly not to millisecond accuracy, so it is natural to take a uniform prior $p(dt) = \text{const}$. Then, the posterior distribution for the time offset is

$$p(dt|s) \propto \exp \left\{ \frac{\rho^2}{2} [\langle h_0|h_0(dt) \rangle^2 + \langle h_{\frac{\pi}{2}}|h_0(dt) \rangle^2] \right\}. \quad (17)$$

At quadratic order, this gives[¶]

$$\langle h_0|h_0(dt) \rangle^2 \approx 1 - dt^2 [\langle \partial_t h_0|\partial_t h_0 \rangle - \langle h_0|\partial_t h_0 \rangle^2] \quad (18)$$

$$\langle h_{\frac{\pi}{2}}|h_0(dt) \rangle^2 \approx dt^2 \langle h_{\frac{\pi}{2}}|\partial_t h_0 \rangle^2. \quad (19)$$

Then, since taking the derivative of the waveform with respect to t_o amounts to multiplication by $2\pi i f$,

$$\langle h_0|h_0(dt) \rangle^2 \approx 1 - 4\pi^2 dt^2 \langle f h_0|f h_0 \rangle = 1 - 4\pi^2 (dt)^2 \overline{f^2}. \quad (20)$$

Here, we have introduced $\overline{f^n}$ to describe the frequency moments of the signal as

$$\overline{f^n} := 4 \int_0^\infty df \frac{|\tilde{h}(f)|^2}{S(f)} f^n. \quad (21)$$

Similarly (19) is approximated as

$$\langle h_{\frac{\pi}{2}}|h_0(dt) \rangle \approx 2\pi \overline{f} dt, \quad (22)$$

where \overline{f} is the mean frequency defined via (21). Thus, at quadratic order, the timing distribution is

$$p(dt|s) \propto \exp [-2\rho^2 \pi^2 \sigma_f^2 dt^2] \quad \text{where} \quad \sigma_f^2 = \overline{f^2} - \overline{f}^2 \quad (23)$$

is the *effective bandwidth* of the signal. In this case, the timing estimator is unbiased and has a width given by

$$\sigma_t = \frac{1}{2\pi\rho\sigma_f}. \quad (24)$$

This is a simple result which encapsulates the expected timing accuracy for a given source. It is inversely proportional to both the signal to noise ratio (SNR) ρ and effective bandwidth σ_f of the source.

[¶] This expression is somewhat different that what is obtained by directly expanding Eq. (17). However, by expanding $\langle h(dt)|h(dt) \rangle = 1$ in powers of dt , it is easy to show that the two expressions are equivalent.

Detector	\bar{f} (Hz)	σ_f (Hz)	σ_t (ms)		Timing accuracy (ms)	
			$\rho = 7$	$\rho = 10$	$\rho = 7$	$\rho = 10$
Initial LIGO	150	100	0.23	0.17	0.27	0.18
Initial Virgo	140	140	0.16	0.11	0.19	0.12
Advanced LIGO	110	120	0.19	0.13	0.21	0.13

Table 1. Timing accuracy for binary neutron stars in different detectors. The table gives the mean frequency and effective bandwidth of the signal. Then, the timing accuracies based on the quadratic approximation (24) and the exact result are given for SNR 7 and 10.

3.3. Example: Binary Coalescence

We can apply the results obtained above to the binary coalescence waveforms of section 2.1. As well as providing a concrete example, it will allow us to investigate the accuracy of the quadratic approximation used to derive Eq. (24) above.

We begin by considering a $1.4 - 1.4M_\odot$ BNS. The values of the mean frequency \bar{f} , effective bandwidth σ_f and timing accuracy σ_t are given in Table 1. Interestingly, all of the detectors have similar mean frequencies and bandwidths with the broad design noise curve of Virgo leading to the largest effective bandwidth. Note that although the frequency bandwidth of Advanced LIGO is not significantly greater than initial LIGO, a signal at the same distance would appear with approximately twelve times the SNR, and therefore the timing accuracy would be fifteen times better. A detailed study of the timing accuracy for various different Advanced LIGO configurations has been investigated in [26].

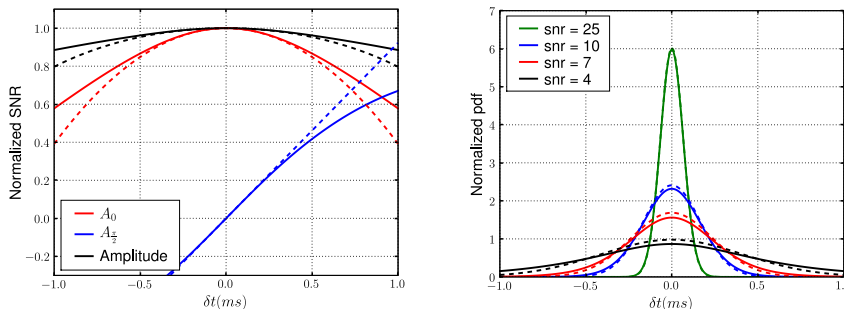


Figure 1. **Left:** The normalized SNR ratio against time for initial LIGO. The SNR for the two phases of the template are plotted, as a function of time, when the waveform has zero phase. The solid lines are the exact results, dotted lines show the SNR approximated using the quadratic approximation discussed in this section. **Right:** The timing distribution for a BNS system at a given SNR in initial LIGO. The dotted lines are the quadratic approximation, while the solid curves are the exact expression. At low SNR, the quadratic approximation underestimates the timing uncertainty.

In Figure 1, we investigate the accuracy of the quadratic approximation used in obtaining (24). The figure shows the SNR as a function of time for initial LIGO, exactly calculated and using the approximation introduced above. In both cases, the masses of the simulated signal and template waveform agree. The quadratic approximation is only good to about 0.5 ms after which it significantly underestimates

Detector	Waveform to ISCO			Full waveform			
	\bar{f} (Hz)	σ_f (Hz)	σ_t (ms) $\rho = 10$	\bar{f} (Hz)	σ_f (Hz)	σ_t (ms) $\rho = 10$	σ_t (ms) $\rho_I = 10$
Initial LIGO	120	40	0.37	150	100	0.16	0.14
Initial Virgo	90	50	0.34	140	140	0.12	0.10
Advanced LIGO	75	50	0.34	120	130	0.11	0.10

Table 2. Timing accuracy based on quadratic approximation for $10 - 10M_\odot$ black hole binary. The results are given for the waveform truncated at the ISCO frequency and for the full waveform based on the phenomenological waveforms of [38]. We give the timing accuracy for signals at SNR 10. The final column shows the timing accuracy for a waveform which accumulates an SNR of 10 to ISCO, if found using the full waveform template.

the recovered SNR. This leads to an underestimation of the timing uncertainty, as shown in the right hand plot. The approximated distributions are more sharply peaked than the exact ones; the timing uncertainty is underestimated by about 20% at a signal SNR of 7, and 15% at SNR of 10. It is only at SNR of 25 or more that the quadratic approximation introduces negligible error.

Finally, consider a $10 - 10M_\odot$ BBH system. Table 2 gives the effective bandwidth and timing accuracy for both post-Newtonian waveforms truncated at ISCO and full, phenomenological waveforms. Interestingly, even though only 15 to 20% additional SNR is accumulated after ISCO, the timing accuracy improves by as much as a factor of three due to the additional high frequency content of the waveform.

4. Sky Localization from Triangulation

Given a timing uncertainty in each of a network of detectors, this can be translated to a localization accuracy for the network. In the previous section, we have derived a simple expression for the timing accuracy for an elliptical waveform as $\sigma_t \approx (2\pi\rho\sigma_f)^{-1}$, where ρ is the observed SNR and σ_f is the effective bandwidth of the signal in the detector. However, much of what follows makes use only of the timing accuracy, without reference to its derivation and would be applicable to other waveform families.

To obtain the timing results, we have assumed that the amplitudes of the two phases of the waveform in each detector are independent. While this is valid for a single detector, for more than two detectors, these amplitudes are not independent since the gravitational wave has only two polarizations. This can be seen in detail for coalescing binaries using a simple counting argument. For three detectors we make 9 measurements (two amplitudes and a time in each), but these are dependent on only 7 parameters ($D, \theta, \phi, \psi, \iota, \phi_o, t_o$). However, it is reasonable to assume that any correlations between observed detector amplitudes will only serve to improve the accuracies derived below.

4.1. Two site network

A two site network will give single measurement of timing differential and will therefore provide only partial localization of the signal. Suppose that the source is located at position \mathbf{R} on the unit sphere, and consider two detectors separated by a distance (expressed in light seconds) of \mathbf{D} . Then, the difference in the time of arrival of the

signal between the two sites is

$$(T_1 - T_2) = \mathbf{D} \cdot \mathbf{R} \quad (25)$$

If the two detectors have timing accuracies σ_1 and σ_2 , the distribution of the observed times t_1 and t_2 is

$$p(t_1, t_2 | s) \propto p(t_1, t_2) \exp \left[-\frac{(t_1 - T_1)^2}{2\sigma_1^2} - \frac{(t_2 - T_2)^2}{2\sigma_2^2} \right]. \quad (26)$$

Localization will depend only upon the time delay ($t_1 - t_2$), so we re-express (26) in terms of a fiducial arrival time and the reconstructed location \mathbf{r} . Marginalizing over the arrival time, with a uniform prior, gives

$$p(\mathbf{r} | \mathbf{R}) \propto p(\mathbf{r}) \exp \left[-\frac{(\mathbf{D} \cdot (\mathbf{r} - \mathbf{R}))^2}{2(\sigma_1^2 + \sigma_2^2)} \right]. \quad (27)$$

As expected, from the timing observation in two detectors, it is only possible to restrict the location of the source in the direction parallel to the separation \mathbf{D} between the detectors. The localization ability is improved by better timing accuracy in the detectors, and also by an increased baseline between detectors.

When localizing a source, we would like to provide the smallest region of the sky which contains the source, with a given confidence. This requires the choice of a prior distribution for the sky location \mathbf{r} . In the absence of directional information,⁺ it is natural to choose the prior on \mathbf{r} to be uniformly distributed on the unit sphere, giving a uniform prior distribution of $\mathbf{D} \cdot \mathbf{r} \in [-1, 1]$. Then, for a 90% confidence region, we obtain

$$\frac{\text{Area}(90\%)}{4\pi} \approx \frac{3.3\sqrt{\sigma_1^2 + \sigma_2^2}}{D}. \quad (28)$$

The area is independent of the location of the signal. For the LIGO detectors $D = 10$ ms so that a timing accuracy of 0.25 ms in each detector limits the signal to about 12% of the sky. For LIGO and Virgo, the light travel time is significantly larger at 27 ms and consequently, with the same timing accuracy, the signal can be localized to about 4% of the sky.

4.2. Three site network

The three detector result can be obtained in a similar manner. As before, we re-express the observed detector arrival times in terms of the reconstructed sky location \mathbf{r} and fiducial arrival time t_0 . Marginalizing over the arrival time gives

$$p(\mathbf{r} | \mathbf{R}) \propto p(\mathbf{r}) \exp \left[-\frac{1}{2}(\mathbf{r} - \mathbf{R})^T \mathbf{M} (\mathbf{r} - \mathbf{R}) \right], \quad (29)$$

where the matrix \mathbf{M} , describing the localization accuracy, is given by

$$\mathbf{M} = \frac{\mathbf{D}_{12}\mathbf{D}_{12}^T}{\sigma_{12}^2} + \frac{\mathbf{D}_{23}\mathbf{D}_{23}^T}{\sigma_{23}^2} + \frac{\mathbf{D}_{31}\mathbf{D}_{31}^T}{\sigma_{31}^2}. \quad (30)$$

⁺ In some cases, it might be reasonable to change this assumption. For example, in many cases it is reasonable to restrict the prior on \mathbf{r} to be localized to nearby galaxies [41]. Alternatively, the detectors' directional sensitivities make it more likely that the signal came from certain sky locations.

Thus \mathbf{M} has a contribution from each pair of detectors which depends upon the detector separation \mathbf{D}_{ij} and the pairwise timing uncertainty

$$\sigma_{ij}^2 = \sigma_i^2 + \sigma_j^2 + \frac{\sigma_i^2 \sigma_j^2}{\sigma_k^2} \quad (31)$$

where $k \neq i, j$. The timing uncertainty from a given pair of detectors is dependent upon the timing accuracy σ_k in the third detector. Initially, this may seem surprising, but arises quite naturally due to the single marginalization over the fiducial arrival time. Finally, we note that the two detector result (26) can be reproduced by taking $\sigma_3 \rightarrow \infty$.

Since the \mathbf{D}_{ij} are coplanar, \mathbf{M} will have a zero eigenvalue and hence a degenerate direction \hat{e}_z normal to this plane. Thus, the three detector network can only restrict the sky location projected onto the plane formed by the detectors. In addition, since \mathbf{M} is independent of the sky location — it depends solely on the location and timing accuracies of the individual detectors — the localization ability *within the plane of the detectors* is independent of the location in that plane. We can complete the coordinate system by introducing co-ordinates \hat{e}_x and \hat{e}_y in eigen-directions of \mathbf{M} . In this basis, the sky localization distribution is

$$p(\mathbf{r}|\mathbf{R}) \propto p(\mathbf{r}) \exp \left[-\frac{1}{2} \left(\frac{(x-X)^2}{\sigma_x^2} + \frac{(y-Y)^2}{\sigma_y^2} \right) \right], \quad (32)$$

where (X, Y) are the co-ordinates of the source, projected onto the plane of the detector and (x, y) describe the recovered location.

As before, we will use this distribution to obtain confidence regions on the sky. The regions will depend upon the prior distribution on \mathbf{r} . Although a uniform distribution on the unit sphere does not lead to a uniform distribution on the $x-y$ plane, in most cases the source localization is sufficiently accurate to treat $p(x, y)$ as constant over this small region; we will make this approximation. In projecting the result back to the sky, we obtain two mirror sky locations ($z \rightarrow -z$) and an additional factor of $(\cos \theta)^{-1}$, where θ is the angle between the line of sight and the normal to the plane of the detectors.* If we assume that the mirror degeneracy can be broken with amplitude consistency tests, the source can be localized with probability p to an area:

$$\text{Area}(p) \approx 2\pi\sigma_x\sigma_y [-\ln(1-p)] / \cos \theta. \quad (33)$$

If the reflection degeneracy cannot be broken then the area is doubled, apart from close to the plane of the detectors in which case the error boxes from the mirror locations will overlap. The best case scenario occurs when the signal is directly overhead the plane of the detectors. The median occurs when $\cos \theta = 1/2$ and gives a factor of two increase in localization area.

To provide a concrete example of expected localization abilities, we consider the LIGO-Virgo network of detectors. The light travel time between the LIGO sites is 10 ms, while between Virgo and the two LIGO sites is around 27 ms for both. Since the two LIGO detectors have similar sensitivities and a very similar orientation, a large fraction of sources will have similar timing uncertainties in the two detectors.

* Of course this breaks down when the source approaches the plane of the detectors, namely $\theta \sim \pi/2$. Close to the plane of the detectors, we can approximate the sky localization by considering the extreme case where the source is in the plane of the detectors, and specifically at $x=1, y=0$. The uncertainty in the y-direction will be proportional to σ_y but in the z-direction, we obtain $\sigma_z \propto \sqrt{\sigma_x}$.

Therefore, we simplify by taking the timing accuracy σ_l of the two LIGO detectors to be identical, but allow the Virgo timing σ_v to differ. Then, the eigen-directions of the matrix \mathbf{M} are roughly aligned with the line connecting the LIGO sites \hat{e}_x and the line connecting its midpoint to Virgo \hat{e}_y and the localization accuracies in these directions are given by

$$\sigma_x \approx \frac{\sigma_l}{7\text{ms}} \quad \text{and} \quad \sigma_y \approx \frac{\sqrt{(2\sigma_v^2 + \sigma_l^2)/3}}{22\text{ms}}. \quad (34)$$

For a 90% confident localization, assuming reflection degeneracy can be broken

$$\text{Area}(90\%, \text{best}) \approx 20 \text{ deg}^2 \left(\frac{\sigma_l}{0.25\text{ms}} \right) \left(\frac{\sqrt{(2\sigma_v^2 + \sigma_l^2)/3}}{0.25\text{ms}} \right) \quad (35)$$

The localization error box is double the size for the median location, $\cos\theta = 1/2$, and will contain two equal size, disconnected pieces if the reflection degeneracy cannot be broken. For the worst case scenario, where the source is in the plane of the detectors, we obtain an error box of over 100 deg^2 for a 0.25 ms timing accuracy. For reference, a 1 deg^2 localization for best and median sources requires timing accuracies of 0.06 ms, 0.04 ms in all detectors.

4.3. Example: Binary Coalescence

Based on the results of recent searches [42], we will take an SNR of 7 in each of the LIGO and Virgo detectors to be the approximate amplitude where a binary coalescence signal would stand above the noise background. For BNS signals of this amplitude Table 1 gives a timing accuracy of 0.27 ms for the LIGO detectors and 0.19 ms for Virgo. This gives at best case localization of 20 deg^2 . A signal would require an SNR of around 25 and a well located source to reduce the 90% localization ellipse to 1 deg^2 — certainly a possibility for the louder sources in the advanced detector era. The localization accuracy for $10 - 10M_\odot$ BBH waveforms is comparable to BNS, namely 20 deg^2 for optimally located signals at single detector SNR of 7. Interestingly, the inclusion of the merger and ringdown portions of the signal provide an order of magnitude improvement in the localization accuracy. This improvement is consistent with what was observed in a detailed study of parameter estimation for BBH [43].

The sensitive band of advanced detectors is expected to begin at around 10 Hz, and it will take a BNS system over a thousand seconds to evolve from 10 Hz to coalescence. Thus, it is interesting to consider the possibility of localizing the source *prior* to detection to allow for early pointing of electromagnetic telescopes. The SNR of the signal $\rho(t)$ will accumulate during the coalescence. Similarly, the frequency will evolve. During the inspiral phase, the frequency of the orbit evolves to leading order as $f(t) \propto (t_o - t)^{-3/8}$ where t_o is taken to as time of coalescence. Thus, making use of (21) and (23) we can calculate the accumulated bandwidth of the signal as a function of time, $\sigma_f(t)$. Using (24), we can investigate how the timing accuracy σ_t evolves during the coalescence.

Figure 2 shows the evolution of the accumulated SNR, frequency bandwidth and timing accuracy over the course of the binary inspiral. While a large fraction of SNR has accumulated 10 seconds before merger, the bandwidth, and consequently the timing accuracy, is largely accrued in the last second prior to merger. Unfortunately, this would seem to make advanced localization of BNS systems unlikely, even with advanced detectors. However, electromagnetic follow-up is still worthwhile as signals

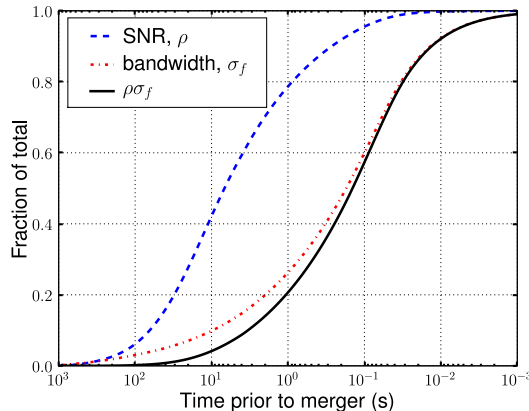


Figure 2. The growth of SNR ρ and signal bandwidth σ_f as a function of time prior to merger. The timing uncertainty $\sigma_t \propto (\rho\sigma_f)^{-1}$ decreases as the binary nears merger. Although a large fraction of the SNR is accumulated well before merger, the bandwidth increases significantly right before merger. Hence, the timing uncertainty is only decreased in the last second or so prior to merger.

associated with coalescing binaries are expected to be emitted after coalescence [44], or be delayed by dispersion through the interstellar medium [45] and therefore arrive after the gravitational wave signal.

5. Systematic Uncertainties

In a gravitational wave search, there are numerous systematic errors associated to the waveform which affect the localization accuracy. In this section, we consider systematic uncertainties due to waveform and calibration errors. These issues have been considered in the context of detectability and parameter estimation accuracy in [46, 47, 48]. Errors in the template waveform might arise due to the breakdown of analytic approximations, or numerical inaccuracies in simulating the waveform. We also consider the effect of calibration errors on localization and show that they can be handled in a very similar manner to waveform errors. However, calibration errors are independent at the different detectors, whereas the waveform errors are not.

5.1. Waveform errors

Let us generalize the analysis introduced in section 3 by allowing for an error in the waveforms used for filtering. Following [49], we write:

$$\tilde{h}_0(f; t_o) = A(f)(1 + \delta a) \exp[2\pi i f t_o + i\Phi(f) + i\delta\phi(f)], \quad (36)$$

where δa and $\delta\phi$ characterize the amplitude and phase errors in the waveform respectively; we continue to assume that $\tilde{h}_{\frac{\pi}{2}}(f; t_o) = i\tilde{h}_0(f; t_o)$. Since δa and $\delta\phi$ are unknown functions of frequency, they cannot be treated with the standard Fisher matrix technology. However we can expand the likelihood in powers of δa and $\delta\phi$ to second order to obtain

$$\ln \Lambda(\delta a, \delta\phi, \delta t) \approx \frac{\rho^2}{2} [1 - \langle h_0(2\pi f \delta t + \delta\phi) | h_0(2\pi f \delta t + \delta\phi) \rangle]$$

$$\begin{aligned}
& + \langle h_0(2\pi f \delta t + \delta\phi) | h_0 \rangle^2 \\
& - \langle h_0(\delta a) | h_0(\delta a) \rangle + \langle h_0(\delta a) | h_0 \rangle^2. \tag{37}
\end{aligned}$$

Interestingly, there are no cross terms between the amplitude and phase errors. Therefore, although the amplitude errors will affect the likelihood they do not have an effect (at leading order) on the timing.

Given a phasing error $\delta\phi$, it is straightforward to differentiate (37) to obtain the timing offset $\hat{\delta t}$ which maximizes the likelihood as

$$\hat{\delta t} = \frac{1}{\sigma_f^2} \left(4 \int_0^\infty df \frac{|\tilde{h}(f)|^2}{S(f)} (\bar{f} - f) \left[\frac{\delta\phi(f)}{2\pi} \right] \right). \tag{38}$$

In general the phasing error $\delta\phi$ is not known explicitly, instead bounds on the maximum error $\delta\phi_{\max}$ are usually provided. In many cases only a maximum phase error is provided, independent of frequency, then the timing offset is bounded by

$$|\hat{\delta t}| \leq \frac{\delta\phi_{\max}}{2\pi\sigma_f^2} \left(4 \int_0^\infty df \frac{|\tilde{h}(f)|^2}{S(f)} |\bar{f} - f| \right), \tag{39}$$

and the bound is only obtained if the phase error is maximal at all frequencies, and changes sign at the mean frequency \bar{f} . Finally, we note that the integrand in (39) gives the mean absolute deviation of the frequency. Since this is always less than or equal to the standard deviation, the timing offset can be bounded by

$$|\hat{\delta t}| \leq \frac{1}{\sigma_f} \left[\frac{\delta\phi_{\max}}{2\pi} \right]. \tag{40}$$

For most realistic phase errors, the uncertainty obtained from (38) will be significantly smaller than (40).

The systematic error ($\hat{\delta t}$ from Eq. (40)) and statistical error (σ_t from Eq. (24)) are directly comparable. Both are inversely proportional to the frequency bandwidth of the signal. The statistical uncertainty is also inversely proportional to the amplitude (or SNR) of the signal, while the systematic is independent of amplitude. Thus, for a phasing error of 5° , the systematic offset is guaranteed to be smaller than the statistical fluctuations for waveforms with an SNR less than 12. In reality, the bound in (40) is rather loose and therefore a 5° phasing error is unlikely to dominate the statistical timing uncertainty at an SNR less than 20.

The same waveform family will be used to search the data from all instruments. Therefore, the waveform error $\delta\phi$ will be the same at all sites. Two detectors will record a different timing offset only if their power spectra (and consequently the mean frequency and effective bandwidth) differ. This immediately argues that between LIGO sites with comparable sensitivities, the timing offset due to a waveform error will be negligible. The timing uncertainty between LIGO and Virgo will depend upon the details of the waveform. Given a specific waveform and phase error, one can evaluate (38) to obtain the results.

5.2. Calibration Errors

Errors in the calibration of the detectors will also affect the timing accuracy. We have denoted the detector output or strain as $s(t)$. This is obtained by calibrating the

detector output $v(t)$ using a response function $R(f)$. This response function is then used to obtain the calibrated data:[50]‡

$$\tilde{s}(f) = R(f)\tilde{v}(f). \quad (41)$$

In a real detector, the response function is time dependent, however we assume that the response function is (approximately) constant over the duration of the signal. In practice, the response function $R_c(f)$ which is calculated will not agree identically with the true response of the instrument. Using the measured response function, the instrumental output is calibrated to obtain the data stream:

$$\tilde{s}_c(f) = R_c(f)\tilde{v}(f) = \frac{R_c(f)}{R(f)}\tilde{s}(f). \quad (42)$$

The errors in calibration will affect signals in the data, as well as the noise and consequently the noise power spectrum, $S(f)$.

To calculate the effect of the calibration errors, we need to evaluate the likelihood (12) obtained when using the incorrect response function. This requires the calculation of both the inner product between signal and template, as well as the template normalization, with the incorrect response function. We will use the notation $\langle \cdot | \cdot \rangle_c$ to denote the existence of calibration errors in the power spectrum used in computing the inner product.

We begin by calculating the effect of calibration errors on the inner product between signal and template:

$$\begin{aligned} \langle s_c | h \rangle_c &= 4 \operatorname{Re} \int df \frac{\left(\frac{R_c(f)}{R(f)} \right) \tilde{s}(f) \tilde{h}^*(f)}{\left| \frac{R_c(f)}{R(f)} \right|^2 S(f)} \\ &= 4 \operatorname{Re} \int df \frac{\tilde{s}(f) \left(\frac{R(f)}{R_c(f)} \tilde{h}(f) \right)^*}{S(f)} = \langle s | h_c \rangle. \end{aligned} \quad (43)$$

where we have introduced an effective waveform error due to calibration as:

$$h_c(f) = \left(\frac{R(f)}{R_c(f)} \right) \tilde{h}(f). \quad (44)$$

Similarly, it is straightforward to show that calibration errors in the calculation of the template norm can be expressed as

$$\langle h | h \rangle_c = \langle h_c | h_c \rangle. \quad (45)$$

Therefore, the calibration errors can be quantified in exactly the same way as the waveform errors discussed in the previous section where

$$(1 + \delta a(f)) \exp[i\delta\phi(f)] = \left(\frac{R(f)}{R_c(f)} \right). \quad (46)$$

This is precisely the form in which calibration errors are expressed, for example in [50].

The timing errors for a given phase accuracy are as given in the previous section. However, as has already been emphasized, the calibration errors are uncorrelated between instruments, so expressions (38-40) are directly applicable.

‡ In practice, the process is generally performed in the time domain to directly produce $s(t)$. However, that will not affect the discussion below as the same systematic uncertainties in calibrating the data still arise.

5.3. Example: Binary Coalescence

Let us return once more to the coalescing binary waveforms and evaluate the effect of waveform uncertainties on the timing. In Figure 3 we plot the integrand of (38) for both the BNS and $10 - 10M_\odot$ BBH signals. The most significant contribution to timing errors arise at frequencies above and below the mean frequency \bar{f} , but where the detector still has good sensitivity. Given a model of the waveform error $\delta\phi(f)$, it can be integrated against the curves in Figure 3 to obtain the timing offset.

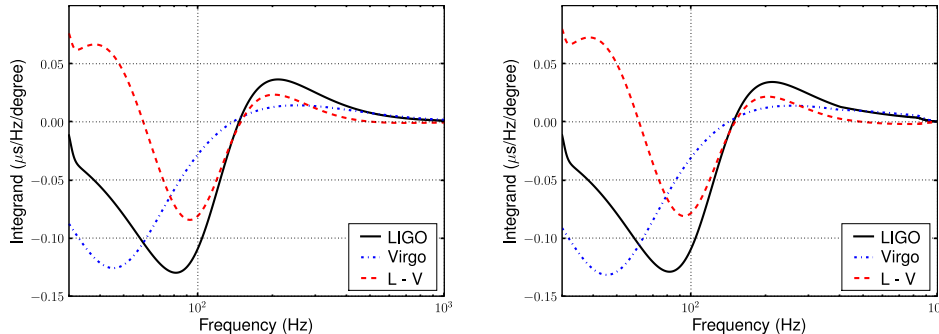


Figure 3. The contribution that different frequencies make to the timing offset given in equation (38). The left hand plot is for the BNS system, the right hand plot is for the full $10 - 10M_\odot$ coalescence waveform. For both the LIGO and Virgo detectors, frequencies far from the mean, but which still contribute to the signal to noise ratio, contribute most significantly. The different shapes are directly dependent on the instrumental noise curves. The final curve shows the contribution to the timing differential as a function of frequency.

To calculate a worst case scenario for a given maximum phase offset $\delta\phi_{\max}$, we take the absolute value of the curves in Figure 3 and integrate. The resultant errors for BNS are:

$$|\delta t_{\text{LIGO}}| \leq \left[\frac{\delta\phi_{\max}}{5^\circ} \right] 0.09\text{ms}, \quad |\delta t_{\text{Virgo}}| \leq \left[\frac{\delta\phi_{\max}}{5^\circ} \right] 0.06\text{ms}. \quad (47)$$

These are limits on timing errors which would result in each detector from a calibration error of this magnitude. The errors would only be achieved in the (rather unrealistic) circumstance where the phase error was $+5^\circ$ up to the mean frequency and then -5° at all frequencies above this.

The use of an incorrect waveform family will introduce a correlated timing error at the different sites. In particular, it will not introduce a timing systematic between the two LIGO sites, since the detectors have the same noise power spectrum. Figure 3 shows the relative timing offset between LIGO and Virgo detectors. It can again be integrated to obtain the maximal timing effect of

$$|\delta t_{\text{LIGO}} - \delta t_{\text{Virgo}}| \leq \left[\frac{\delta\phi_{\max}}{5^\circ} \right] 0.05\text{ms} \quad (48)$$

For the BBH waveform, the 5° errors are slightly larger at 0.09 ms for LIGO, 0.07 ms for Virgo and 0.05 ms between LIGO and Virgo.

It is illustrative to compare these systematic errors to the statistical timing uncertainties derived in Section 3. In the worst case scenario, a calibration uncertainty

Single Det SNR	Waveform Error (°)	Calibration Error (°)	Timing (ms)		Median 90% Localization (deg ²)
			LIGO	Virgo	
7	-	-	0.27	0.21	40
7	10	10	0.32	0.26	60
7	20	20	0.45	0.38	120
10	-	-	0.18	0.13	17
10	5	5	0.20	0.15	22
10	10	10	0.25	0.20	36
25	-	-	0.06	0.05	2
25	5	5	0.16	0.11	6
25	10	10	0.19	0.13	20

Table 3. Timing and localization accuracy for binary neutron star systems in the LIGO-Virgo network for a range of single detector SNRs and calibration and waveform uncertainties. The intrinsic timing uncertainties are added in quadrature with the calibration and waveform uncertainties. The localization area is calculated from timing information, with the additional assumption that amplitude consistency can break the reflection degeneracy. For an ideally located source (orthogonal to the plane of the detectors) the localization area is half the median value. The numbers are given for the initial/enhanced network; advanced detectors would yield around a 20% improvement in timing and 40% in localization for the same SNR.

in phase of 15° would introduce an error equivalent to the inherent timing uncertainty at (single detector) SNR of 7. Since the waveform errors will not affect the timing between LIGO sites, they can be effectively absorbed into the Virgo timing accuracy, in which case 20° waveform uncertainties will produce comparable uncertainties to inherent timing errors at SNR 7.

Since the waveform, calibration and statistical uncertainties in timing are independent, it is natural to add them in quadrature. For a signal at SNR 7 and 10° waveform and calibration errors, we obtain $\sigma_l \leq 0.32\text{ms}$ for LIGO and $\sigma_v \leq 0.25\text{ms}$ for Virgo. This leads to a 50% degradation of the localization accuracy, so that for ideally located sources the area of the 90% confidence localization ellipse increases to 30deg^2 , and for an average source to 60deg^2 . Table 3 provides the localization accuracies for sample of SNRs and waveform/calibration uncertainties.

6. Discussion

We have introduced a simple method to compute the timing accuracy in a gravitational wave detector and, using this, derived an expression for the localization ability for a network of detectors. For an elliptically polarized waveform, we obtain a timing accuracy of $\sigma_t \approx 1/(2\pi\rho\sigma_f)$. Thus, the timing accuracy scales inversely with both the amplitude and “effective bandwidth” of the signal. For reference, at a signal to noise ratio of 7, the timing accuracy for low mass coalescing binary signals is around 0.25 ms. This holds for both BNS and low mass BBH, although for the latter it is only by considering the full coalescence waveform that this accuracy can be achieved.

For a given timing accuracy in a network of detectors, we have calculated the accuracy with which the source can be localized on the sky. The localization accuracy depends upon the timing accuracy in each of the detectors, the network geometry and the angle between the plane of the detectors and the signal location. A detector

network with widely separated detectors affords the best localization ability, and signals which are normal to the plane of a three detector network are localized with the greatest accuracy. The 90% localization ellipse for an optimally oriented source, with timing accuracy 0.25 ms, in the LIGO–Virgo network has an area of 20 deg^2 . This is doubled for the median location, and doubled again if the reflection degeneracy in the plane of the detectors cannot be broken by other considerations, such as amplitude consistency.

The expressions for localization accuracy derived here could easily be extended to a network of more than three detectors. Although the precise form of the localization distribution has not been calculated, it would be similar in form to the three detector expression (29). In concurrence with other works (e.g. [51]) this argues that additional detectors would most improve localization efforts by providing a large baseline between the new detector and existing LIGO–Virgo network, as well as breaking the reflection symmetry by lying well away from the plane formed by the LIGO–Virgo network.

We have given detailed expressions for the effect of systematic errors on localization. The effects of waveform and calibration uncertainties is almost identical in a single detector. However, the waveform errors will be correlated across the detectors in the network, while calibration errors will not. Due to the similar sensitivity curves of the two LIGO detectors, waveform uncertainties will have little effect on localization, while they will effect the LIGO–Virgo network. Calibration errors will be independent at the different sites and therefore might have a larger effect on localization. We have obtained a bound on the timing error due to calibration errors as $\hat{\delta}t \leq (\delta\phi_{\text{max}}/2\pi\sigma_f)$. By comparing with the inherent timing uncertainty, we see that calibration uncertainty will not dominate provided $\delta\phi_{\text{max}} \leq 1/\rho$. Note, however, that only for a very specific, and unlikely, form of the calibration error will the timing offset be anything like this large.

In this paper, we have not considered the effect of the mismatch between waveform and template parameters. This will surely degrade the localization accuracy which has been derived. However, as for waveform error, the similarity of the LIGO detectors' sensitivities means that waveform errors will have produce negligible timing effect between them, as has been observed in [52]. Furthermore, in [53, 54], it has been argued that the effect of parameter uncertainties can be minimized by choosing an appropriate reference time. In the future, we plan to investigate the effect that parameter mismatch has on timing accuracies, as well as exploring in greater detail the effect of waveform and calibration errors for multi-detector parameter estimation.

There are numerous simplifications and approximations which are made in this paper. While the basic results derived here are qualitatively correct, the detailed expressions for sky localization ellipses will surely be modified as these assumptions are relaxed. For example, if the components of the binary are spinning, then the orbital plane will precess during the evolution, whence the waveform will not be elliptically polarized. However, since the precession will be slow relative to the gravitational wave frequency, it is reasonable to expect that the results will be similar in the case of spinning binaries. Likewise, the inclusion of higher waveform harmonics [55, 56] will increase the effective bandwidth of the signals; however it will also require a generalization of the techniques described here to correctly incorporate these signals.

Finally, we note that the localization estimates derived here are based solely on triangulation between sites. Thus, we have neglected significant correlations which must be present in the observed signal at more than two sites. For three sites, there is an amplitude consistency requirement that arises from the fact that the gravitational

waveform has only two polarizations. Amplitude consistency should, in many cases, serve to break the reflection degeneracy that arises by considering triangulation alone and, in obtaining our most optimistic localization results, we have assumed this is the case. It is unlikely that amplitude consistency will further restrict the location. However, as has been emphasized by Searle [57], for a network of three or more detectors, there is also a phase consistency between the observed waveform at the sites. For an elliptically polarized waveform observed in two sites, there is always an orientation and polarization such that the observed phase difference is consistent with a given sky location. However, for three sites, this is no longer the case and phase consistency can be used to further restrict possible locations. Any phasing requirement will naturally give a timing accuracy inversely proportional to the signal's mean frequency \bar{f} . Thus, in the case where the mean frequency is significantly larger than the bandwidth, one obtains higher frequency oscillations (from phasing) on top of the slower falloff (from timing alone). This will lead to improvements in localization, and would be interesting to investigate further. However, for coalescing binaries, the mean frequency and bandwidth are comparable which suggests this will not be a significant effect.

Acknowledgements

We would like to thank many people for interesting discussions on this topic, in particular John Baker, Duncan Brown, Kipp Cannon, Lee Lindblom, Larry Price, Bangalore Sathyaprakash, Anthony Searle and Chris Van Den Broeck. We thank Patrick Sutton for many detailed discussions and comments on the paper draft, and Ray Frey for detailed comments on the paper draft. This research was made possible thanks to support from the Royal Society.

References

- [1] Schutz B F 1986 *Nature* **323** 310–311
- [2] Stamatikos M, Gehrels N, Halzen F, Meszaros P and Roming P W A 2009 (*Preprint arXiv:0902.3022[astro-ph.HE]*)
- [3] Prince T A *et al.* 2009 (*Preprint arXiv:0903.0103[astro-ph.CO]*)
- [4] Bloom J S *et al.* 2009 (*Preprint arXiv:0902.1527[astro-ph.CO]*)
- [5] Phinney E S 2009 (*Preprint arXiv:0903.0098[astro-ph.CO]*)
- [6] Nakar E 2007 *Phys. Rept.* **442** 166–236 (*Preprint astro-ph/0701748*)
- [7] Abbott B *et al.* (LIGO Scientific) 2008 *Phys. Rev.* **D77** 062004 (*Preprint arXiv:0709.0766[gr-qc]*)
- [8] LIGO Scientific Collaboration and Hurley K 2008 *Astroph. Journal* **681** 1419–1430 (*Preprint arXiv:0711.1163v2[astro-ph]*)
- [9] Abbott B *et al.* (LIGO Scientific) 2008 *Phys. Rev. Lett.* **101** 211102 (*Preprint arXiv:0808.2050[astro-ph]*)
- [10] Abbott B *et al.* (LIGO Scientific) 2009 (*Preprint arXiv:0905.0005[astro-ph.HE]*)
- [11] Pan-starrs <http://pan-starrs.ifa.hawaii.edu/public/>
- [12] Swift <http://swift.gsfc.nasa.gov/docs/swift/swiftsc.html>
- [13] Fermi <http://fermi.gsfc.nasa.gov/>
- [14] Antares <http://antares.in2p3.fr/>
- [15] Fender R *et al.* 2006 *PoS MQW6* 104 (*Preprint astro-ph/0611298*)
- [16] Icecube <http://icecube.wisc.edu/>
- [17] Lofar <http://www.lofar.org/>
- [18] Dhurandhar S V and Tinto M 1988 In Perth 1988, Proceedings, Recent developments in theoretical and experimental general relativity, gravitation and relativistic field theories, pt. B 1811- 1814.
- [19] Gürsel Y and Tinto M 1989 *Phys. Rev. D* **40** 3884–3938

- [20] Searle A C, Sutton P J, Tinto M and Woan G 2008 *Class. Quant. Grav.* **25** 114038 (*Preprint arXiv:0712.0196[gr-qc]*)
- [21] Searle A C, Sutton P J and Tinto M 2009 *Class. Quant. Grav.* **26** 155017 (*Preprint arXiv:0809.2809[gr-qc]*)
- [22] Cavalier F *et al.* 2006 *Phys. Rev.* **D74** 082004 (*Preprint gr-qc/0609118*)
- [23] Wen L, Fan X and Chen Y 2008 *Journal of Physics: Conference Series* **122** 012038 (7pp) URL <http://stacks.iop.org/1742-6596/122/012038>
- [24] Beauville F *et al.* 2006 *J. Phys. Conf. Ser.* **32** 212 (*Preprint gr-qc/0509041*)
- [25] Birindelli S 2008 *Coherent algorithm for reconstructing the location of a coalescing binary using a system of three gravitational wave interferometers* Ph.D. thesis University of Pisa
- [26] King A and Cannon K 2008 Whitened Merger-Waveform Autocorrelation Functions: Implications for Inspiral Event Localization in Advanced LIGO Tech. Rep. LIGO-T080312-00
- [27] Markowitz J, Zanolin M, Cadonati L and Katsavounidis E 2008 *Physical Review D (Particles, Fields, Gravitation, and Cosmology)* **78** 122003 (pages 11) URL <http://link.aps.org/abstract/PRD/v78/e122003>
- [28] Sutton P and Poprocki S *Private Communication*
- [29] Brady P R and Fairhurst S 2008 *Class. Quant. Grav.* **25** 1050002 (*Preprint arXiv:0707.2410[gr-qc]*)
- [30] Allen B, Anderson W G, Brady P R, Brown D A and Creighton J D E 2005 Findchirp: an algorithm for detection of gravitational waves from inspiraling compact binaries (*Preprint arXiv:gr-qc/0509116*) URL <http://www.citebase.org/abstract?id=oai:arXiv.org:gr-qc/0509116>
- [31] Blanchet L 2002 *Living Rev. Rel.* **4** 3 (*Preprint arXiv:gr-qc/0202016*)
- [32] Pretorius F 2005 *Phys. Rev. Lett.* **95** 121101 (*Preprint gr-qc/0507014*)
- [33] Campanelli M, Lousto C O, Marronetti P and Zlochower Y 2006 *Phys. Rev. Lett.* **96** 111101 (*Preprint gr-qc/0511048*)
- [34] Baker J G, Centrella J, Choi D I, Koppitz M and van Meter J 2006 *Phys. Rev. Lett.* **96** 111102 (*Preprint gr-qc/0511103*)
- [35] Pretorius F 2009 Binary black hole coalescence *Physics of Relativistic Objects in Compact Binaries: from Birth to Coalescence* ed Colpi M, Casella P, Gorini V, Moschella U and Possenti A (Heidelberg, Germany: Springer) (*Preprint arXiv:0710.1338[gr-qc]*)
- [36] Husa S 2007 *Eur. Phys. J. ST* **152** 183–207 (*Preprint arXiv:0812.4395[gr-qc]*)
- [37] Hannam M 2009 Status of black-hole-binary simulations for gravitational-wave detection (*Preprint arXiv:0901.2931[gr-qc]*)
- [38] Ajith P *et al.* 2007 *Class. Quant. Grav.* **24** S689–S699 (*Preprint arXiv:0704.3764[gr-qc]*)
- [39] Maggiore M Oxford University Press, October 2007. 572p. (ISBN-13: 978- 0-19-857074-5)
- [40] Jaynes E T 2003 *Probability Theory: The Logic of Science (Vol 1)* (Cambridge University Press) ISBN 0521592712
- [41] Kopparapu R K, Hanna C, Kalogera V, O’Shaughnessy R, Gonzalez G, Brady P R and Fairhurst S 2008 *Astrophys. J.* **675** 1459–1467
- [42] Abbott B *et al.* (LIGO Scientific) 2009 Search for Gravitational Waves from Low Mass Binary Coalescences in the First Year of LIGO’s S5 Data (*Preprint 0901.0302*)
- [43] Ajith P and Bose S 2009 (*Preprint arXiv:0901.4936[gr-qc]*)
- [44] Nakar E 2007 *Phys. Rep.* **442** 166–236 (*Preprint arXiv:astro-ph/0701748v1*)
- [45] Lorimer D R, Bailes M, McLaughlin M A, Narkevic D J and Crawford F 2007 (*Preprint arXiv:0709.4301[astro-ph]*)
- [46] Lindblom L, Owen B J and Brown D A 2008 *Phys. Rev.* **D78** 124020 (*Preprint arXiv:0809.3844[gr-qc]*)
- [47] Lindblom L 2009 (*Preprint arXiv:0907.0457[gr-qc]*)
- [48] Lindblom L 2009 (*Preprint 0906.5153*)
- [49] Allen B 1996 LIGO calibration accuracy Tech. Rep. LIGO-T960189-00-Z LIGO Project URL <http://www.ligo.caltech.edu/docs/T/T960189-00.pdf>
- [50] Dietz A, Garofoli J, González G, Landry M, O’Reilly B and Sung M 2006 Calibration of the LIGO detectors for S4 Tech. Rep. LIGO-T050262-01-D LIGO Project URL <http://www.ligo.caltech.edu/docs/T/T050262-01.pdf>
- [51] Blair D G *et al.* 2008 *J. Phys. Conf. Ser.* **122** 012001
- [52] Aylott B *et al.* 2009 *Class. Quant. Grav.* **26** 165008 (*Preprint arXiv:0901.4399[gr-qc]*)
- [53] Beauville F *et al.* (LIGO / Virgo working group) 2008 *Class. Quant. Grav.* **25** 045001 (*Preprint gr-qc/0701027*)
- [54] Acernese F *et al.* 2007 *Class. Quant. Grav.* **24** S617–S625
- [55] Van Den Broeck C 2006 *Class. Quant. Grav.* **23** L51–L58 (*Preprint gr-qc/0604032*)

- [56] Van Den Broeck C and Sengupta A S 2007 *Class. Quant. Grav.* **24** 155–176 (*Preprint gr-qc/0607092*)
- [57] Searle A *Private Communication*